Desalination and Water Treatment
www.deswater.com

doi: 10.5004/dwt.2020.24816

174 (2020) 106–115
January

Removal efficiency and adsorption kinetics of perfluorohexanoic acid by MgAl-carbonate layered double hydroxide and its calcined products

Yuechao Wu, Yulin Wang, Jiangguang Li, Jiale Dai, Wangjia Lu, Mingping He, Zhengqiang Dong, Wanli Xu, Liang Lv*

College of Chemical and Materials Engineering, Quzhou University, Zhejiang 324000, China, emails: Lianglv_qzxy@126.com (L. Lv), wuyuechao112@aliyun.com (Y.-C. Wu), csu_lin@163.com (Y.-L. Wang), 13867020905@163.com (J.-G. Li), daijiale1999@aliyun.com (J.-L. Dai), hnlwj8170309@163.com (W.-J. Lu), hemingping1985@163.com (M.-P. He), gaocaidzq@163.com (Z.-Q. Dong), xuwanli0525@163.com (W.-L. Xu)

Received 20 March 2019; Accepted 24 August 2019

ABSTRACT

In this study, perfluorohexanoic acid (PFHxA) was presented as pollutant in water and magnesium-aluminum-carbonate layered double hydroxide (MgAl-LDH) as well as its calcined product (CLDH) were presented as sorbents. The physical and chemical properties of as-prepared MgAl-LDH and CLDH were examined by Fourier transform infrared (FT-IR) analysis, X-ray diffraction analysis, Brunauer–Emmett–Teller (BET) analysis and X-ray photoelectron spectroscopy analysis. The FT-IR results indicated that the as-prepared samples are the desired products and the structure of CLDH has recovered after adsorption of PFHxA. The X-ray diffraction (XRD) analysis confirmed that the synthesized products have well-ordered layer structure and PFHxA can be removed from aqueous solution through entering interlayer of CLDH. The BET analysis verified the surface areas and pore size distributions of MgAl-LDH and CLDH, respectively. The X-ray photoelectron spectroscopy (XPS) analysis further proved the adsorption mechanism via element changes between CLDH before and after adsorption. For the adsorption experiment, the effects of the adsorption conditions including calcination, dosage, temperature and duration of oscillation have been investigated. The best removal efficiency of PFHxA by CLDH is 89.54%, which is provided by 0.1 g CLDH at 65°C for 30 min in 30 mL PFHxA solution with initial concentration of 0.3592 g/L. The adsorption kinetics of PFHxA by CLDH was studied. The kinetic data were well-fitted to the pseudo-first-order kinetic model. Based on FT-IR and kinetic analysis, the "memory effect" may play an important role in adsorption stage. Since CLDH show excellent removal efficiency of PFHxA, they are expected to separate PFHxA from water in pollution control.

Keywords: PFHxA; MgAl-LDH; CLDH; Removal efficiency; Adsorption kinetics

1. Introduction

As one of the rapid-developing chemicals, perfluorohexanoic acid (PFHxA) exhibits promising potential applications in industrial fields and human daily life, such as carpets, paper and non-stick cookware, for their high stability and special surface activity [1–4]. On the other hand, due to prohibitive energy between covalent caobon-fluorine bonds as well as deficiency of active groups, PFHxA can not only be transported and diffused in various ambient medium, but also can be taken-in and accumulated in animals, eventually terminate in human body through food chains or other pathway [5,6]. Consequently, the extensive utilization of PFHxA in many fields such as textiles, chemicals, pharmaceuticals and so on has resulted in ever-increasing harm for health and environment [7,8].

---

* Corresponding author.

1944-3994/1944-3986

In order to explore simple and effective as well as environmental friendly treatment for PFHxA, multiple methods have been attempted, such as adsorption [9,10], photochemical degradation, nanofiltration [11,12], sonolysis [13–16], anodizing and biodegradation [17–20]. However, most techniques are of embarrassingly low removal efficiency or produce secondary pollution to the environment. As the most effective and convenient treatment for PFHxA, adsorption has been receiving a lot of attention. As a matter of fact, substantial types of absorbents have been published, 3D graphene oxide–based composites [21–23], modified alumina [24,25], Fe_3O_4-based composites [26–28], graphene/nanotubes [29,30], layered double hydroxides (LDHs) based composites [31–33] and so on. In this work, LDHs have been chosen as adsorbent for the treatment of PFHxA.

As one kind of typical anionic intercalation material, LDHs, whose backbones are composed of metal hydroxides, show great potential in removal of PFHxA in wastewater due to their unique lamellar construction [34–37]. The basic chemical formula of LDHs is defined as $[M^{2+}_{1-x}M^{3+}_{x}(OH)_2]^{x+}(A^{n-}_{x/n})\cdot yH_2O$, where M^{2+} represents divalent cation while M^{3+} represents trivalent cation, which are held in octahedral positions between hydroxide layers, A^{n-} is an exchangeable anion, and x is the ratio of $M^{3+}/(M^{2+} + M^{3+})$. The type of M^{2+} and M^{3+} as well as the ratio of M^{2+}/M^{3+} are adjustable on the basis of actual conditions. Moreover, after calcinated at 450°C–500°C, LDHs with CO_3^{2-} group can be turned into layered double oxides, which possess relatively larger specific surface area as well as air porosity and remain lamellar structure with disappearance of exchangeable anions. After contact with anionic solution, construction of layered double oxides can be recovered to the original organized lamellar structure, which is known as "memory effect" [38].

Various compositions of LDHs have been widely proposed as potential adsorbents, for instance, Zhang et al. [31] synthesized LiAl-LDH through coprecipitation with removal efficiency of 11.8%–97.26% for fluoride. Wang et al. [32] synthesized MgAl-LDHs@MoS_2 and showed removal efficiency for Cr(VI) in aqueous solutions from 15.3% to 50.6%. MgAl-LDH-coated hollow carbon microsphere composites were synthesized through hydrothermal method by Wang et al. [32], and the removal efficiency was from 0% to 96% for Pb(II) and from 15% to 97% for humid acid [39].

Compared with other pollution, such as fluoride [31], heavy metals [32,39,40], dye [33], 2-chlorophenol [41], organic indicators [42,43], it is noticed that the removal of PFHxA by application of LDHs is limited. Thus in this paper, we have innovatively investigated the influencing factors on removal efficiency of PFHxA in aqueous solution by MgAl-CO_3 LDHs (MgAl-LDH) and CLDH (calcination of MgAl-LDH), respectively. Also, the kinetics during adsorption process and reusability of CLDH after adsorption have been examined for further research.

2. Experimental section

2.1. Materials

$Mg(NO_3)_2\cdot 6H_2O$, $Al(NO_3)_3\cdot 9H_2O$, NaOH, Na_2CO_3 are analytically pure reagents and used without further purification. All the water used was deionized and decarbonated.

2.2. Synthesis of MgAl-LDH and CLDH

MgAl-LDH sample was acquired through co-precipitation method [34,44]. The mixed solution of NaOH and Na_2CO_3 was prepared as precipitant and the nitrates were dissolved in deionized water according to molar ratio of $n_{Mg}:n_{Al} = 3:1$. Under constant and intensive stirring, solution of precipitant was added dropwise into mixed solution of $Mg(NO_3)_2\cdot 6H_2O$ and $Al(NO_3)_3\cdot 9H_2O$ at 65°C and pH = 10. After stirring for 18 h, raw products were subsequently treated through crystallization, centrifugation, cleansing and drying.

CLDH sample was obtained after calcination of as-prepared MgAl-LDH at 450°C for 6 h.

2.3. Description of PFHxA standard curve

In order to acquire PFHxA standard curve, which explain the relationship between solution concentration, aqueous solution of PFHxA with initial concentration of 0.3592 g/L was diluted to a series of standard solution with concentration of 0.1796, 0.08980, 0.07184, 0.03592, 0.01796, 0.008980, and 0.003592 g/L, respectively, then the standard curve between concentration and intensity can be described as $y = 1.3000 \times 10^6 x + 2{,}708$ ($R^2 = 0.9999$).

2.4. Investigation of influencing factors to remove PFHxA

In this work, we have studied factors such as calcination, dosage, duration and temperature of oscillation on PFHxA removal efficiency. Several series of PFHxA aqueous solution were adsorbed under different univariate, respectively. The concentration of PFHxA after adsorbing can be calculated according to standard curve in section 2.3.

2.4.1. Calcination

Comparison of PFHxA removal efficiency by MgAl-LDH and CLDH was carried out under temperature of 45°C. 0.1 g MgAl-LDH and CLDH were added into 30 mL PFHxA solution with initial concentration of 0.1796 g/L, respectively. The oscillatory process was monitored by HPLC and would not be suspended until the signal intensity tested by HPLC was essentially kept steady.

2.4.2. Dosage of CLDH

A series of 30 mL PFHxA solution with initial concentration of 0.1796 g/L was treated by 0.05, 0.075, 0.10, 0.15 and 0.20 g CLDH at 45°C, respectively. The oscillating process was monitored by HPLC and would be terminated while the signal intensity tested by HPLC essentially kept steady.

2.4.3. Temperature of oscillation

A series of 30 mL PFHxA solution with initial concentration of 0.1796 g/L was treated by 0.1 g CLDH, respectively. After oscillating at 25°C, 35°C, 45°C, 55°C and 65°C for 10 min, respectively, the samples were detected by HPLC.

2.4.4. Duration of oscillation

0.1 g CLDH was added into 30 mL PFHxA solution with initial concentration of 0.1796 g/L and then the mixture was oscillated at 65°C. Samples for HPLC detection were taken at 1, 2, 3, 4, 5, 6, 8, 10, 15, 20, 30 and 60 min, respectively.

2.5. Investigation of kinetics

For the sake of further understanding in adsorption mechanism, kinetics has been explored in this paper as well.

0.1 g CLDH was added into 30 mL PFHxA solution with initial concentration of 0.1796 g/L and oscillated at 25°C. Samples for HPLC detection were taken at 1, 2.5, 5, 10, 15, 20, 25, 30, 4, 50, 60, 75, 90, 120 and 150 min, respectively. The steps above were repeated at 35°C, 45°C, 55°C and 65°C, respectively.

2.6. Investigation of layer-anions exchange in CLDH after adsorption

The displacements of Cl^-, HCO_3^-, CO_3^{2-}, SO_4^{2-} and NO_3^- with CLDH, which has achieved adsorption equilibrium in PFHxA solution, respectively, have been investigated in this part.

0.1 g CLDH that has achieved adsorption equilibrium in PFHxA solution at 45°C was dissolved in HCl solution, which was then adjusted to neutral by NaOH solution. After that, deionized water was added into the mixture solution until volume was up to 30 mL. This as-prepared solution was finally detected by HPLC to obtain the initial signal intensity.

Under temperature of 45°C, a series of 30 mL NaCl, $NaHCO_3$, Na_2CO_3, Na_2SO_4 and $NaNO_3$ solution with initial anionic concentration of 0.1 mol/L was treated by 0.1 g CLDH that has achieved adsorption equilibrium in PFHxA solution at 45°C, respectively. Samples for HPLC detection were taken at 5, 10, 15, 30, 60 and 90 min, respectively.

2.7. Investigation of regeneration and reutilization of CLDH after adsorption

It is necessary and essential to regenerate CLDH after adsorption for reutilization. Na_2CO_3 solution with concentration of 0.1 mol/L was prepared for regeneration of CLDH after adsorption, then MgAl-LDH can be regenerated from the exchange of CO_3^{2-} and CLDH after adsorption. After washed and dried, the sample was calcined at 450°C for 6 h. The regenerated sample was then taken as adsorbent for five repeated trials.

3. Results and discussion

3.1. Characterization of MgAl-LDH and CLDH

3.1.1. FT-IR

FT-IR analysis was adopted to study structural differences among MgAl-LDH, CLDH before adsorption and CLDH after adsorption; results are shown in Fig. 1.

The three peaks near 3,500 cm^{-1} in three curves, respectively, represent for stretching vibration of hydroxyl group, the three peaks near 1,650 cm^{-1} in three curves, respectively, are bending vibrations of hydroxyl group, the three peaks near 1,380 cm^{-1} in three curves, respectively, are characteristic peaks for carbonate, the three peaks near 650 cm^{-1} in three curves, respectively, are lattice vibration for bonds between metal and oxide.

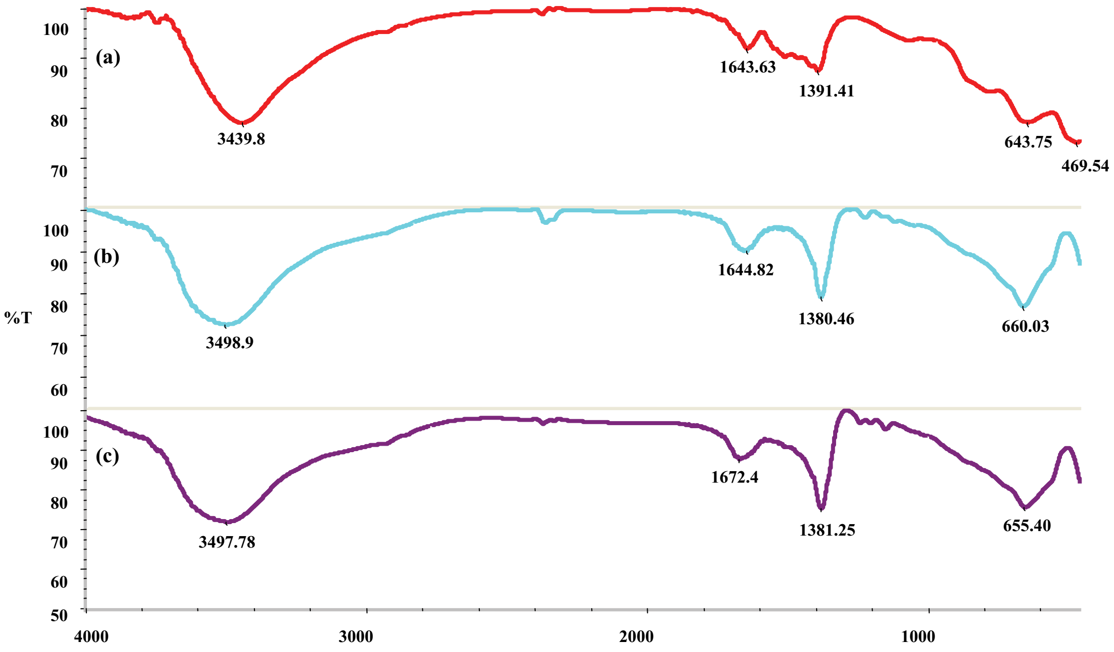

Fig. 1. FT-IR spectra of (a) CLDH before adsorption; (b) MgAl-LDH; (c) CLDH after adsorption.

By comparison of three curves in Fig. 1, the peaks near 3,500 and 1,380 cm^{-1} of CLDH before adsorption is obviously smaller than that of MgAl-LDH, respectively, which indicate that hydroxyl group and carbonate in MgAl-LDH are released partially during calcination. On the other hand, the curve of CLDH after adsorption is almost similar to that of MgAl-LDH, which is mainly caused by CO_2 gas dissolved in PFHxA solution enter into interlayer of CLDH.

In Fig. 2, after displacement of NO_3^- with CLDH, the peak near 1,380 cm^{-1} is obviously sharpened, which maybe contributed from entrance of NO_3^- into interlayer of CLDH. In curve (c), due to existence of CO_3^{2-} between layers of CLDH, the peak near 1,380 cm^{-1} is broadened. In curve (d), the novel peak emerging at 1,122 cm^{-1} is characteristic for SO_4^{2-}. All of the phenomena verify that the exchange of anions in CLDH is realized by entrance of anions.

3.1.2. X-ray diffraction

In order to study the changes in structures, MgAl-LDH, CLDH before adsorption and CLDH after adsorption have been tested by XRD. Fig. 3 shows the results. In curve A, the strong peaks, which are of sharp and symmetrical shapes, appearing at 11.7°, 22.6°, 34.4° and 59.5° are corresponding to classic diffracted signal of LDHs. Therefore, it is definitely that the as-prepared product is MgAl-LDH. At the same time, the disappearance of peaks at 11.7°, 22.6° and 34.4° in curve B indicating disappearance of CO_3^{2-} and H_2O between layers of CLDH before adsorption. In contrast to curve B, the peaks at 11.7°, 22.6° and 34.4° are recovered in curve C on account of memory effect. This recovery substantially demonstrates that PFHxA can be removed from aqueous solution through entering interlayer of CLDH.

3.1.3. BET analysis

The surface areas and pore size distributions of MgAl-LDH and CLDH were investigated by Brunauer–Emmett–Teller (BET) analysis, respectively. Results are summarized in Table 1. Apparently, CLDH has larger specific surface area and pore volume as well as smaller average pore diameter,

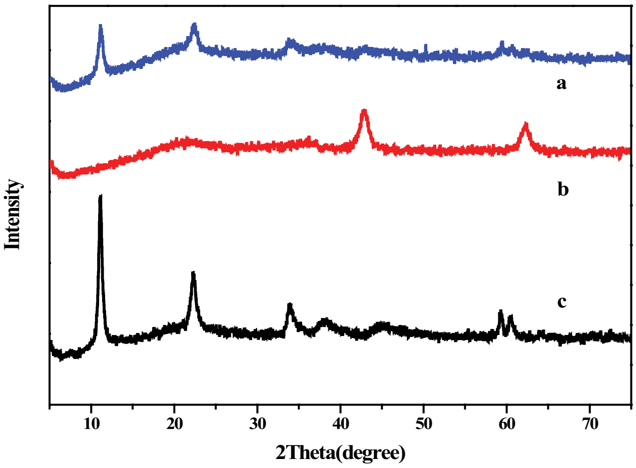

Fig. 3. XRD spectra of (a) MgAl-LDH; (b) CLDH before adsorption; (c) CLDH after adsorption.

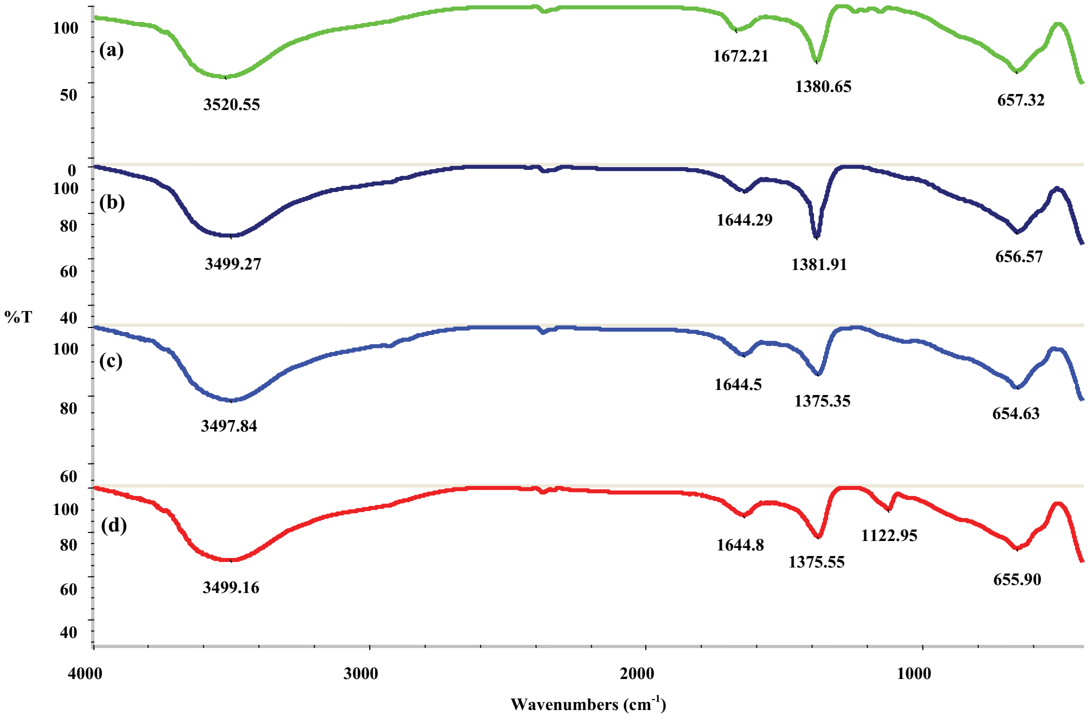

Fig. 2. FT-IR spectra of (a) CLDH after adsorption; (b) displacement of NO_3^- with CLDH; (c) displacement of CO_3^{2-} with CLDH; (d) displacement of SO_4^{2-} with CLDH.

resulting in its excellent removal efficiency of PFHxA. This phenomenon was caused by destruction of the brucite-like layers and formation of the porous structure in the interlayer of CLDH during the calcination process.

3.1.4. XPS analysis

In order to further demonstrate the adsorption mechanism, XPS analysis was adopted to reveal the element changes between CLDH before and after adsorption. Figs. 4 and 5 show the results. It has been confirmed that the existence of major elements (Mg, Al, O, C) in samples. The peak of Na 1s in CLDH before adsorption was from the precipitant in the synthesis of MgAl-LDH, and then disappeared in CLDH after adsorption. Notably, there is an obvious peak of F 1s as the form of C-F and C-F_2 in CLDH after adsorption, which is corresponding to the results of XRD analysis, testifying that PFHxA can enter interlayer of CLDH.

Table 1
Physical structures of MgAl-LDH and CLDH

Sample	MgAl-LDH	CLDH
BET surface area (m^2/g)	65.67	171.1
Pore volume (cm^3/g)	0.2158	0.4592
Average pore diameter (nm)	13.15	10.73

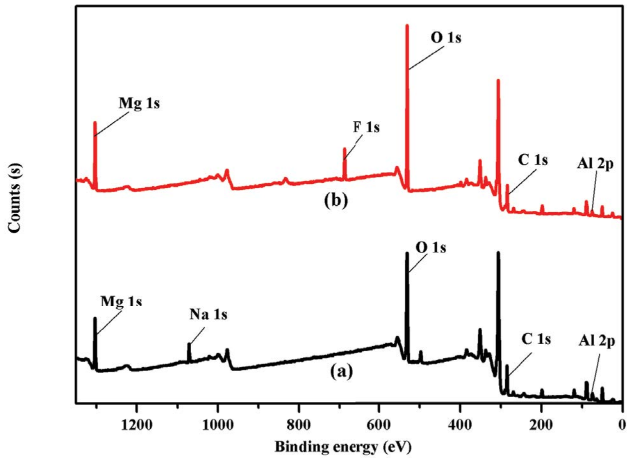

Fig. 4. XPS spectra of (a) CLDH before adsorption; (b) CLDH after adsorption.

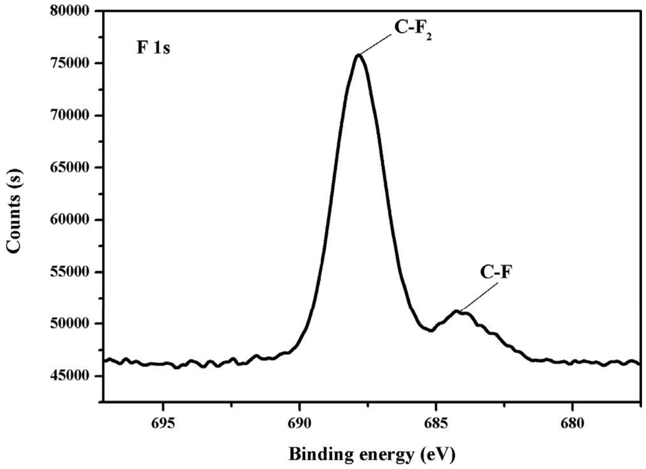

Fig. 5. XPS spectrum of F 1s.

3.2. Influence factors on removal efficiency of PFHxA by MgAl-LDH and CLDH

3.2.1. Influence of calcination

Results are shown in Fig. 6. Apparently, in both curves, the removal efficiency of PFHxA virtually kept stable when duration of oscillation reaches 60 min. In addition, the removal efficiency of PFHxA by CLDH is obviously better than removal efficiency of PFHxA by MgAl-LDH, for example, removal efficiency of PFHxA by CLDH can achieve 79.32% at 90 min while that of PFHxA by MgAl-LDH can hardly come up to 20.04%. The results are in consonance with the test of BET. On the basis of this investigation, CLDH would be the preference for the following experiments.

3.2.2. Influence of dosage

Fig. 7 exhibits the results. The removal efficiency of PFHxA improves undoubtedly as the increase of dosage, especially for dosage of 0.10, 0.15 and 0.20 g, however, removal efficiency by dosage of 0.10 g is almost the same as removal efficiency by dosage of 0.15 g. On the other hand, compared with that by dosage of 0.10 and 0.15 g the removal efficiency by dosage of 0.20 g is slightly declining, which might be caused by agglomeration from excessive CLDH. In conclusion, dosage of 0.10 g is the optimum dosage for the following experiments.

3.2.3. Influence of temperature of oscillation

The relationship between temperature of oscillation and removal efficiency of PFHxA is shown in Fig. 8. Generally

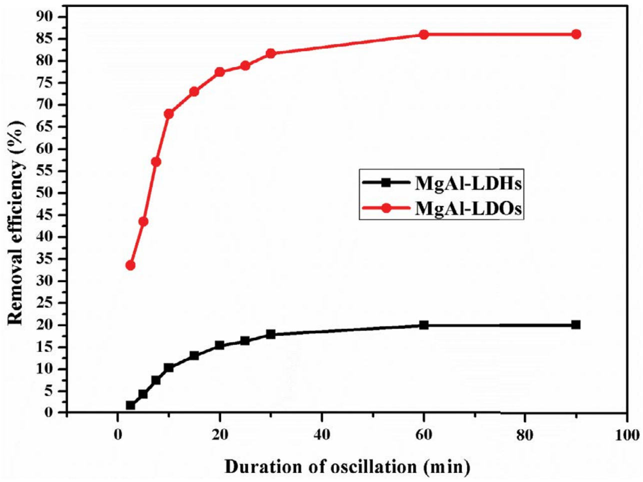

Fig. 6. Influence of calcination on removal efficiency of PFHxA ($V = 30$ mL, $T = 45$°C, $w_{\text{MgAl-LDH}} = 0.1$ g, $w_{\text{CLDH}} = 0.1$ g, $C_0 = 0.1796$ g/L).

speaking, higher temperature is favorable for elevating removal efficiency of PFHxA. And the optimal removal efficiency of PFHxA achieves 81.10% when temperature of oscillation reaches 65°C. Hence, 65°C is adopted for investigating influence of duration of oscillation.

3.2.4. Influence of duration of oscillation

Results are exhibited in Fig. 9. The removal efficiency of PFHxA raises sharply until duration of oscillation reaches 15 min. After that the growth of removal efficiency tends to be gentle and almost terminated at 30 min for removal efficiency of 87.52%.

3.3. Adsorption kinetics of PFHxA by CLDH

The experimental and calculated data are exhibited in Fig. 10. Subsequently, calculation by Eq. (1) was taken out to acquire the data in Table 2 for nonlinear-fitting by pseudo-first-order kinetic model (Eq. (2)) and pseudo-second-order kinetic model (Eq. (3)), respectively. Results are shown in Figs. 11 and 12.

$$q_t = \frac{(C_0 - C_t)V}{m} \tag{1}$$

In Eq. (1) q_t is adsorption quantity during t time. C_0 and C_t are concentrations of PFHxA solution at initial time and concentration of PFHxA solution at t time, respectively, V is for volume of PFHxA solution, m is dosage of LDHs.

$$\frac{dq_t}{dt} = k_1(q_e - q_t) \tag{2}$$

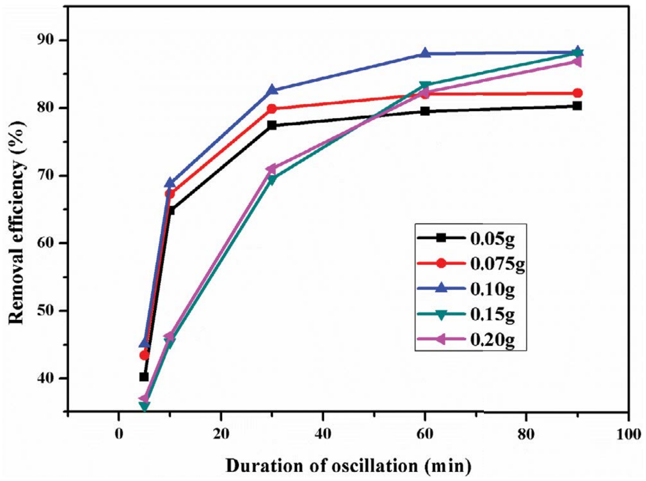

Fig. 7. Relationship between dosage of CLDH and removal efficiency of PFHxA (V = 30 mL, T = 45°C, C_0 = 0.1796 g/L).

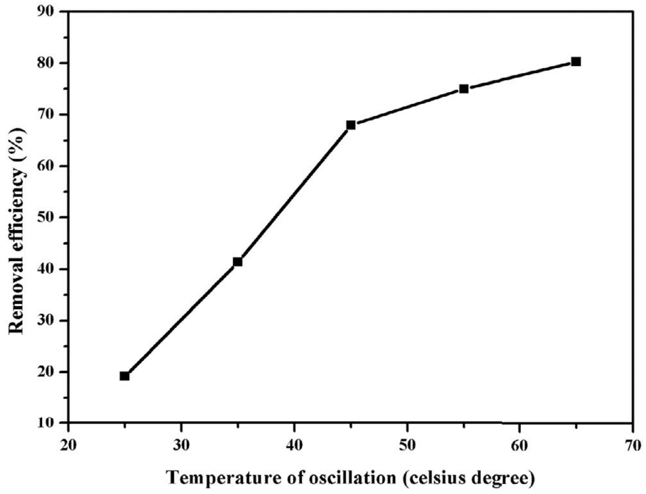

Fig. 8. Relationship between temperature of oscillation and removal efficiency of PFHxA (V = 30 mL, w_{CLDH} = 0.1 g, C_0 = 0.1796 g/L).

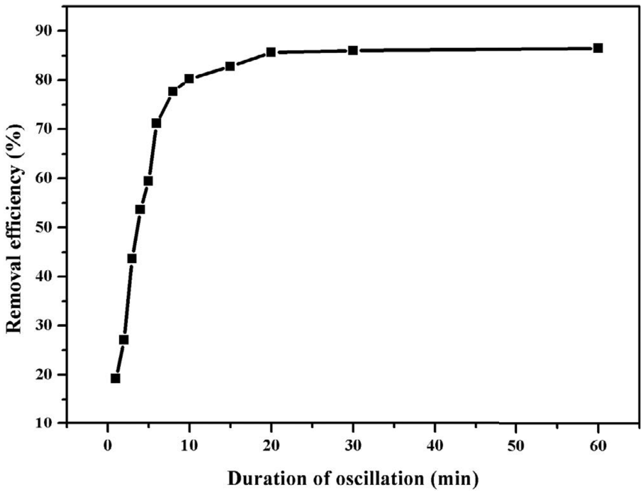

Fig. 9. Relationship between duration of oscillation and removal efficiency of PFHxA (V = 30 mL, T = 65°C, w_{CLDH} = 0.1 g, C_0 = 0.1796 g/L).

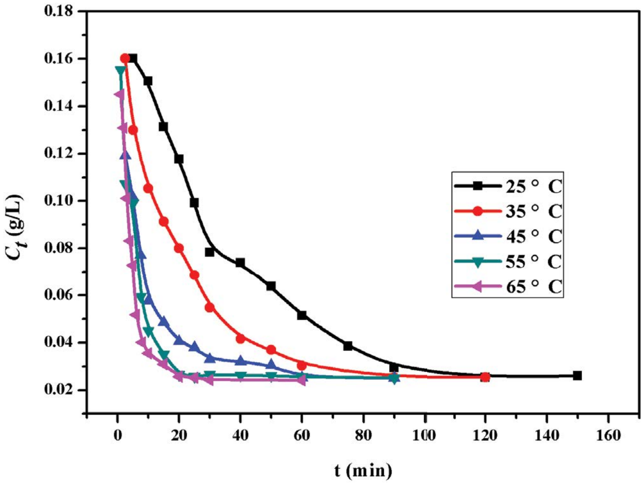

Fig. 10. Experimental data and calculated data for adsorption kinetics of PFHxA by CLDH (V = 30 mL, w_{CLDH} = 0.1 g, C_0 = 0.1796 g/L).

Table 2
Data for nonlinear-fitting of adsorption kinetics of PFHxA by CLDH

Duration of oscillation (min)	q_t (mmol/g)				
	25°C	35°C	45°C	55°C	65°C
5	0.0185	0.0474	0.0747	0.0769	0.1020
10	0.0277	0.0710	0.1166	0.1287	0.1376
15	0.0462	0.0843	0.1252	0.1380	0.1421
20	0.0591	0.0951	0.1329	0.1463	0.1470
25	0.0768	0.1060	0.1353	0.1471	0.1475
30	0.0967	0.1194	0.1401	0.1464	0.1484
40	0.1009	0.1318	0.1410	0.1465	0.1485
50	0.1107	0.1363	0.1425	0.1467	0.1486
60	0.1226	0.1426	0.1475	0.1472	0.1485
90	0.1436	0.1474	0.1477	0.1476	0.1485
120	0.1473	0.1473	0.1475	0.1476	0.1486

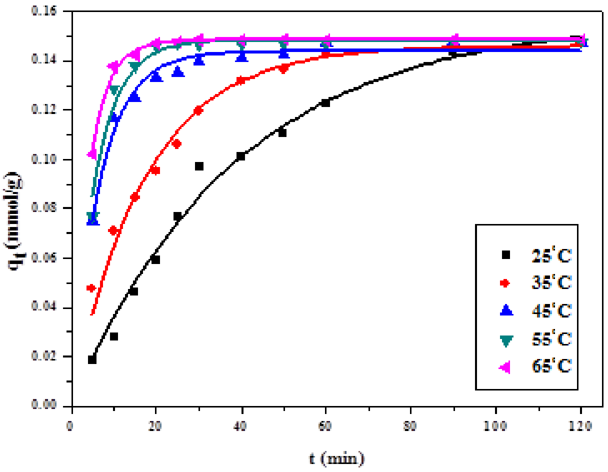

Fig. 11. Nonlinear-fitting curves by pseudo-first-order kinetic model.

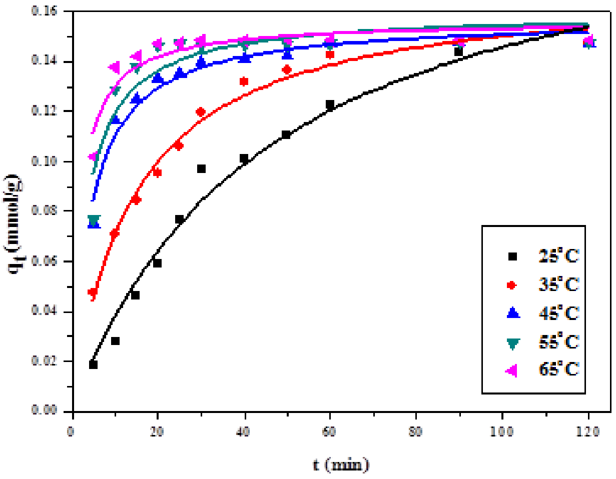

Fig. 12. Nonlinear-fitting curves by pseudo-second-order kinetic model.

$$\frac{dq_t}{dt} = k_2(q_e - q_t)^2 \tag{3}$$

In Eqs. (2) and (3) q_t and q_e are adsorption quantity during t time and adsorption quantity in equilibrium, respectively. t is for time while k_1 and k_2 are for pseudo-first-order adsorption rate constant and pseudo-second-order adsorption rate constant, respectively.

It is obvious that the experimental data can be finely fitted by both models. All the parameters obtained through experiments and calculations are listed in Table 3. By comparison of $q_{e,\text{cal}}$ and R^2, it can be found that the adsorption kinetics of PFHxA by CLDH is better described by pseudo-first-order kinetic model. Then Arrhenius equation (Eq. (4)) is introduced to provide activation energy (E_a), the values of ln k_1 and $1/T$ are listed in Table 4 and the relationship between ln k_1 and $1/T$ are illustrated in Fig. 13. From corresponding slope $-(E_a/R)$, E_a can be calculated as 47.04 kJ/mol.

$$\ln k_1 = -\frac{E_a}{R}\frac{1}{T} + \ln A \tag{4}$$

Furthermore, it is observed in Table 5 that the CLDH prepared in this work exhibiting a reasonably high adsorption quantity for PFHxA compared with some of the reported literature [25,26,29,30,45,46] concerned on removal of fluoride. Although there are several adsorbents showing higher adsorption quantity than the as-prepared CLDH, those adsorbents required tedious synthetic works.

3.5. Layer-anions displacement in CLDH

Results are shown in Fig. 14.

In conclusion, the displacement ratios with all five anions are appreciable, especially with NO_3^-, whose displacement equilibrium is achieved at 60 min with ratio of 99%. On the other hand, with displacement ratio of 75.08%, CO_3^{2-} shows displacement equilibrium at 90 min.

3.6. Reusability of CLDH after adsorption

Results are shown in Fig. 15. We could see that the removal efficiency of CLDH decreased from 65.52% to 47.72% after five repeated trials. This might be explained that adsorbed PFHxA was not completely removed during washing which leads to partial blockage of the active sites on CLDH.

4. Conclusion

To sum up, MgAl-LDH and CLDH have been successfully synthesized through coprecipitation method. PFHxA standard curve depicted the relationship between concentration of PFHxA solution and signal intensity of HPLC through HPLC analysis. The results from FT-IR analysis and XRD analysis point out structural differences among MgAl-LDH, CLDH before adsorption and CLDH after adsorption as well as existence of memory effect. The results

Table 3
Experimental conditions, kinetic parameters and statistic parameters for the two kinetic models

C_0 of PFHxA (mmol/L)	Temperature (°C)	$q_{e,\text{exp}}$ (mmol/g)	Pseudo-first-order			Pseudo-second-order		
			$q_{e,\text{cal}}$ (mmol/g)	$k_1 \times 10^{-2}$ (min^{-1})	R^2	$q_{e,\text{cal}}$ (mmol/g)	k_2 (g/mmol min)	R^2
0.5719	25	0.147	0.157	2.59	0.985	0.213	0.101	0.978
0.5719	35	0.147	0.146	5.82	0.988	0.171	0.410	0.985
0.5719	45	0.148	0.144	14.78	0.969	0.157	1.19	0.951
0.5719	55	0.147	0.148	17.02	0.965	0.159	1.85	0.813
0.5719	65	0.148	0.148	23.78	0.991	0.156	3.22	0.853

Table 4
Values of ln k_1 and $1/T$

$1/T$	$\ln k_1$
0.00335	–3.65
0.00325	–2.84
0.00314	–1.91
0.00305	–1.77
0.00296	–1.44

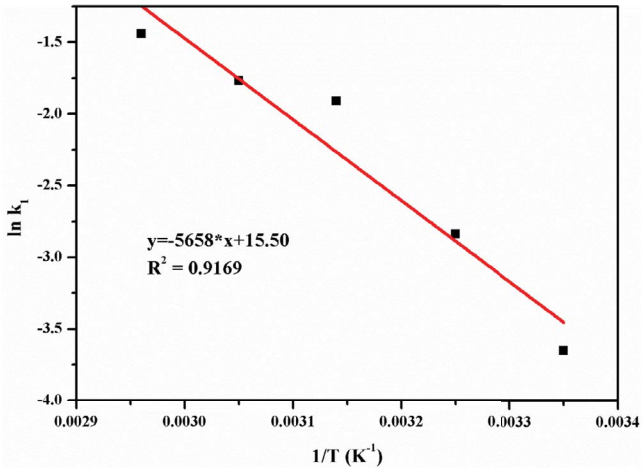

Fig. 13. Arrhenius plots for adsorption of PFHxA by CLDH.

Table 5
Comparison of the adsorption quantities of the as-prepared CLDH with some reported adsorbents

Adsorbents	Adsorption quantity (mg/g)
ZnAl-LDH	4.16
Calcined LiAl-LDH	158.7
Graphene	17.65
Fe_3O_4 nanocomposite	9.43
Organic acid modified mesoporous alumina	47.2–62.5
Hydroxyapatite/multiwalled carbon nanotubes	39.22
CLDH in this work	46.16

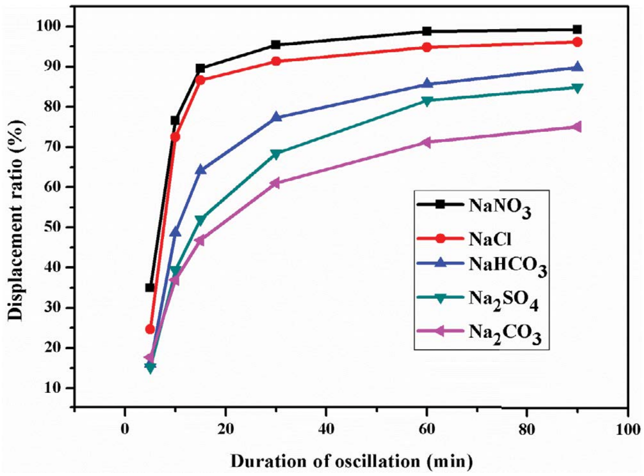

Fig. 14. Intuitive exhibition of displacement ratio with various anions (V = 30 mL, T = 45°C, w_{CLDH} = 0.1 g, C_0 = 0.1 mol/L).

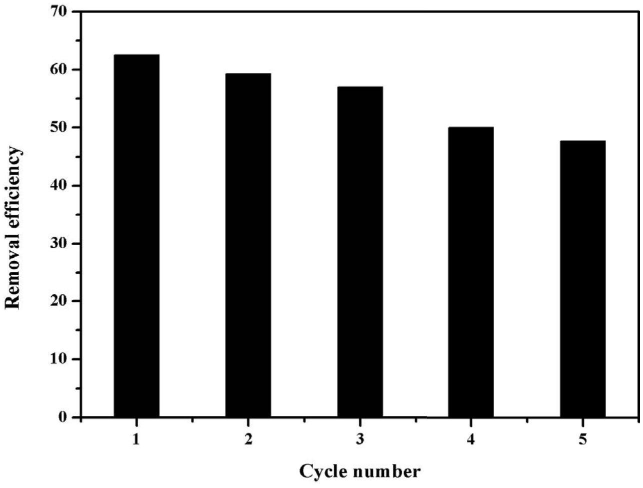

Fig. 15. Recycling of CLDH in the removal of PFHxA (V = 30 mL, T = 25°C, w_{CLDH} = 0.1 g, C_0 = 0.1796 g/L, t = 120 min).

from BET indicate destruction of the brucite-like layers and formation of the porous structure in the interlayer of CLDH during the calcination process. The results from XPS confirm that PFHxA can enter interlayer of CLDH in the form of C-F and C-F_2.

The best removal efficiency of PFHxA by CLDH is 89.54%, which is provided by 0.1 g CLDH at 65°C for 30 min in 30 mL PFHxA solution with initial concentration of 0.3592 g/L. Whereas the removal efficiency already reaches 85.88% at 25°C with 0.1 g CLDH in 30 mL 0.1796 g/L PFHxA for 120 min. The displacement ratios with various anions can be ranked as $NO_3^- > Cl^- > HCO_3^- > SO_4^{2-} > CO_3^{2}$. The displacement ratio with NO_3^- is 99% while that with CO_3^{2-} is only 75.08%. The removal efficiency of CLDH decreased from 65.52% to 47.72% after five repeated trials.

Acknowledgements

This work was partially supported by the National Natural Science Foundation (2127116, 21476127, U1607119), the Public Technology Research Program of Zhejiang Province (GF18B060002, 2015C33231), the Scientific and Technological Fund from Quzhou Science and Technology Bureau (2014Y009, 2016D003, 2017G05, 2017T04), the Domestic Visitor Professional Development Project (FX2014104), the financial support from start-up grant (Quzhou University).

Symbols

A — Pre-exponential factor
C_0 — Concentration of PFHxA solution at initial time
C_t — Concentration of PFHxA solution at t time
E_a — Activation energy
k_1 — Pseudo-first-order adsorption rate constant
k_2 — Pseudo-second-order adsorption rate constant
m — Dosage of LDHs
q_e — Adsorption quantity in equilibrium
q_t — Adsorption quantity during t time
T — Absolute temperature
R — Molar gas constant
t — Reaction time
V — Volume of PFHxA solution

References

[1] S. Vaalgamaa, A.V. Vähätalo, N. Perkola, S. Huhtala, Photochemical reactivity of perfluorooctanoic acid (PFOA) in conditions representing surface water, Sci. Total Environ., 409 (2011) 3043–3048.

[2] S. Fujii, S. Tanaka, N.P.H. Lien, Y. Qiu, C. Polprasert, New POPs in the water environment: distribution, bioaccumulation and treatment of perfluorinated compounds-a review paper, J. Water Supply, 56 (2007) 313–326.

[3] E.F. Houtz, C.P. Higgins, J.A. Field, D.L. Sedlak, Persistence of perfluoroalkyl acid precursors in AFFF-impacted groundwater and soil, Environ. Sci. Technol., 47 (2013) 8187–8195.

[4] K. Prevedouros, I.T. Cousins, R.C. Buck, S.H. Korzeniowski, Sources, fate and transport of perfluorocarboxylates, Environ. Sci. Technol., 40 (2006) 32–44.

[5] K. Kannan, L. Tao, E. Sinclair, S.D. Pastva, D.J. Jude, J.P. Giesy, Perfluorinated compounds in aquatic organisms at various trophic levels in a Great Lakes food chain, Arch. Environ. Contam. Toxicol., 48 (2005) 559–566.

[6] J.M. Conder, R.A. Hoke, W. de Wolf, M.H. Russell, R.C. Buck, Are PFCAs bioaccumulative? A critical review and comparison with regulatory criteria and persistent lipophilic compounds, Environ. Sci. Technol., 42 (2008) 995–1003.

[7] T. Chen, L. Zhang, J. Yue, Z. Lv, W. Xia, Y. Wan, Y. Li, S. Xu, Prenatal PFOS exposure induces oxidative stress and apoptosis in the lung of rat off-spring, Reprod. Toxicol., 33 (2012) 538–545.

[8] L. Mhadhbi, D. Rial, S. Pérez, R. Beiras, Ecological risk assessment of perfluorooctanoic acid (PFOA) and perfluorooctanesulfonic acid (PFOS) in marine environment using *Isochrysis galbana, Paracentrotus lividus, Siriella armata* and *Psetta maxima*, J. Environ. Monit., 14 (2012) 1375–1382.

[9] S.M. Bartell, A.M. Calafat, C. Lyu, K. Kato, P. Barry Ryan, K. Steenland, Rate of decline in serum PFOA concentrations after granular activated carbon filtration at two public water systems in Ohio and West Virginia, Environ. Health Persp., 118 (2010) 222.

[10] S. Deng, Y. Nie, Z. Du, Q. Huang, P. Meng, B. Wang, G. Yu, Enhanced adsorption of perfluorooctane sulfonate and perfluorooctanoate by bambooderived granular activated carbon, J. Hazard. Mater., 282 (2014) 150–157.

[11] C.Y. Tang, Q.S. Fu, A.P. Robertson, C.S. Criddle, J.O. Leckie, Use of reverse osmosis membranes to remove perfluorooctane sulfonate (PFOS) from semiconductor wastewater, Environ. Sci. Technol., 40 (2006) 7343–7349.

[12] C.Y. Tang, Q.S. Fu, C.S. Criddle, J.O. Leckie, Effect of flux (transmembrane pressure) and membrane properties on fouling and rejection of reverse osmosis and nanofiltration membranes treating perfluorooctane sulfonate containing wastewater, Environ. Sci. Technol., 41 (2007) 2008–2014.

[13] F. Hao, W. Guo, A. Wang, Y. Leng, H. Li, Intensification of sonochemical degradation of ammonium perfluorooctanoate by persulfate oxidant, Ultrason. Sonochem., 21 (2014) 554–558.

[14] S. Rayne, K. Forest, Perfluoroalkyl sulfonic and carboxylic acids: a critical review of physicochemical properties, levels and patterns in waters and wastewaters, and treatment methods, J. Environ. Sci. Health, 44 (2009) 1145–1199.

[15] C.D. Vecitis, H. Park, J. Cheng, B.T. Mader, M.R. Hoffmann, Enhancement of perfluorooctanoate and perfluorooctanesulfonate activity at acoustic cavitation bubble interfaces, J. Phys. Chem. C, 112 (2008) 16850–16857.

[16] C.D. Vecitis, Y. Wang, J. Cheng, H. Park, B.T. Mader, M.R. Hoffmann, Sonochemical degradation of perfluorooctanesulfonate in aqueous filmforming foams, Environ. Sci. Technol., 44 (2009) 432–438.

[17] L.M. Colosi, R.A. Pinto, Q. Huang, W.J. Weber Jr, Peroxidase mediated degradation of perfluorooctanoic acid, Environ. Toxicol. Chem., 28 (2009) 264–271.

[18] H.F. Schroder, Determination of fluorinated surfactants and their metabolites in sewage sludge samples by liquid chromatography with mass spectrometry and tandem mass spectrometry after pressurised liquid extraction and separation on fluorine-modified reversed-phase sorbents, J. Chromatogr. A, 1020 (2003) 131–151.

[19] J. Liu, S.M. Avendano, Microbial degradation of polyfluoroalkyl chemicals in the environment: a review, Environ. Int., 61 (2013) 98–114.

[20] B.M. Allred, J.R. Lang, M.A. Barlaz, J.A. Field, Physical and biological release of poly-and perfluoroalkyl substances (PFASs) from municipal solid waste in anaerobic model landfill reactors, Environ. Sci. Technol., 49 (2015) 7648–7656.

[21] X. Xu, J. Zou, X. Zhao, X. Jiang, F. Jiao, J. Yu, Q. Liu, J. Teng, Facile assembly of three-dimensional cylindrical egg white embedded graphene oxide composite with good reusability for aqueous adsorption of rare earth elements, Colloid Surf., A, 570 (2019) 127–140.

[22] X. Zhao, X. Xu, J. Teng, N. Zhou, Z. Zhou, X. Jiang, F. Jiao, J. Yu, Three-dimensional porous graphene oxide-maize amylopectin composites with controllable pore-sizes and good adsorption-desorption properties: facile fabrication and reutilization, and the adsorption mechanism, Ecotoxicol. Environ. Saf., 176 (2019) 11–19.

[23] X. Zhao, X. Xu, X. Jiang, J. Teng, J. Yu, Facile fabrication of three-dimensional and recyclable graphene oxide-melamine composites with high removal efficiency, Desal. Wat. Treat., 148 (2019) 188–194.

[24] X. Ding, Y. Hua, Y. Chen, C. Zhang, X. Kong, Heavy metal complexation of thiol-containing peptides from soy glycinin hydrolysates, Int. J. Mol. Sci., 16 (2015) 8040–8058.

[25] S. Kundu, I.H. Chowdhury, P.K. Sinha, M.K. Naskar, Effect of organic acid-modified mesoporous alumina toward fluoride ions removal from water, J. Chem. Eng. Data, 62 (2017) 2067–2074.

[26] A. Mohseni-Bandpi, B. Kakavandi, R.R. Kalantary, A. Azari, A. Keramati, Development of a novel magnetite-chitosan composite for the removal of fluoride from drinking water: adsorption modeling and optimization, RSC Adv., 5 (2015) 73279–73289.

[27] C. Zhang, Y. Li, T. Wang, Y. Jiang, H. Wang, Adsorption of drinking water fluoride on a micron-sized magnetic Fe_3O_4@ Fe-Ti composite adsorbent, Appl. Surf. Sci., 363 (2016) 507–515.

[28] Y. Zhang, X. Lin, Q. Zhou, X. Luo, Fluoride adsorption from aqueous solution by magnetic core-shell Fe_3O_4@alginate-La particles fabricated via electro-coextrusion, Appl. Surf. Sci., 389 (2016) 34–45.

[29] Y. Li, P. Zhang, Q. Du, X. Peng, T. Liu, Z. Wang, Y. Xia, W. Zhang, K. Wang, H. Zhu, D. Wu, Adsorption of fluoride from aqueous solution by graphene, J. Colloid Interface Sci., 363 (2011) 348–354.

[30] Z. Ruan, Y. Tian, J. Ruan, G. Cui, K. Iqbal, A. Iqbal, H. Ye, Z. Yang, S. Yan, Synthesis of hydroxyapatite/multi-walled carbon nanotubes for the removal of fluoride ions from solution, Appl. Surf. Sci., 412 (2017) 578–590.

[31] T. Zhang, Q. Li, H. Xiao, H. Lu, Y. Zhou, Synthesis of Li-Al layered double hydroxides (LDHs) for efficient fluoride removal, Ind. Eng. Chem. Res., 51 (2012) 11490–11498.

[32] J. Wang, P. Wang, H. Wang, J. Dong, W. Chen, X. Wang, S. Wang, T. Hayat, A. Alsaedi, X. Wang, Preparation of molybdenum disulfide coated Mg/Al layered double hydroxide composites for efficient removal of chromium(VI), ACS Sustain. Chem. Eng., 5 (2017) 7165–7174.

[33] H. Gao, R. Cao, X. Xu, S. Zhang, J. Xue, T. Hayat, N.S. Alharbi, J. Li, Surface area- and structure-dependent effects of LDH for highly efficient dye removal, ACS Sustain. Chem. Eng., 7 (2019) 905–915.

[34] J.S. Valente, J. Hernandez-Cortez, M.S. Cantu, G. Ferrat, E. Lopez-Salinas, Calcined layered double hydroxides Mg-Me-Al´(Me: Cu, Fe, Ni, Zn) as bifunctional catalysts, Catal. Today, 150 (2010) 340–345.

[35] S. He, Y. Zhao, M. Wei, D.G. Evans, X. Duan, Fabrication of hierarchical layered double hydroxide framework on aluminum foam as a structured adsorbent for water treatment, Ind. Eng. Chem. Res., 51 (2011) 285–291.

[36] Q. Zhao, Z. Chang, X. Lei, X. Sun, Adsorption behavior of thiophene from aqueous solution on carbonate- and dodecylsulfateIntercalated ZnAl layered double hydroxides, Ind. Eng. Chem. Res., 50 (2011) 10253–10258.

[37] M. Dadwhal, M. Sahimi, T.T. Tsotsis, Adsorption isotherms of Arsenic on conditioned layered double hydroxides in the presence of various competing ions, Ind. Eng. Chem. Res., 50 (2011) 2220–2226.

[38] Z. Gao, K. Sasaki, X. Qiu, Structural memory effect of Mg–Al and Zn–Al layered double hydroxides in the presence of different natural humic acids: process and mechanism, Langmuir, 34 (2018) 5386–5395.

[39] S. Huang, S. Song, R. Zhang, T. Wen, X. Wang, S. Yu, W. Song, T. Hayat, A. Alsaedi, X. Wang, Construction of layered double hydroxides/hollow carbon microsphere composites and its applications for mutual removal of Pb(II) and humic acid from aqueous solutions, ACS Sustain. Chem. Eng., 5 (2017) 11268–11279.

[40] H. Lu, Z. Zhu, H. Zhang, J. Zhu, Y. Qiu, L. Zhu, S. Küppers, Fenton like catalysis and oxidation/adsorption performances of acetaminophen and arsenic pollutants in water on a multi-metal Cu-Zn-Fe-LDH, ACS Appl. Mater. Interfaces, 8 (2016) 25343–25352.

[41] Y. Chuang, Y. Tzou, M. Wang, C. Liu, P. Chiang, Removal of 2-chlorophenol from aqueous solution by Mg/Al layered double hydroxide (LDH) and modified LDH, Ind. Eng. Chem. Res., 47 (2008) 3813–3819.

[42] C. Jing, Y. Chen, X. Zhang, X. Guo, X. Liu, B. Dong, F. Dong, X. Zhang, Y. Liu, S. Li, Y. Zhang, Low carbonate contaminative and ultrasmall NiAl LDH prepared by acid salt treatment with high adsorption capacity of methyl orange, Ind. Eng. Chem. Res., 58 (2019) 11985–11998.

[43] Q. Wang, X. Wang, C. Shi, LDH Nanoflower lantern derived from ZIF-67 and its application for adsorptive removal of organics from water, Ind. Eng. Chem. Res., 57 (2018) 12478–12484.

[44] S. Britto, P.V. Kamath, Polytypism in the Lithium−Aluminum layered double hydroxides: the $[LiAl_2(OH)_6]^+$ layer as a structural synthon, Inorg. Chem., 50 (2011) 5619–5627.

[45] S. Mandal, S. Mayadevi, Adsorption of fluoride ions by Zn-Al layered double hydroxides, Appl. Clay Sci., 40 (2008) 54–62.

[46] J. Zhou, Y. Cheng, J. Yu, G. Liu, Hierarchically porous calcined lithium/aluminum layered double hydroxides: facile synthesis and enhanced adsorption towards fluoride in water, J. Mater. Chem., 21 (2011) 19353–19361.